Insight into a hexanuclear cobalt complex: Strategy to construct efficient catalysts for visible light-driven water oxidation

Junqi Lin[a], Xiangyu Meng[a], Min Zheng[a], Baochun Ma[a,*], Yong Ding[a,b,*]

[a] State Key Laboratory of Applied Organic Chemistry, Key Laboratory of Nonferrous Metal Chemistry and Resources Utilization of Gansu Province, College of Chemistry and Chemical Engineering, Lanzhou University, Lanzhou, 730000, China
[b] State Key Laboratory for Oxo Synthesis and Selective Oxidation, Lanzhou Institute of Chemical Physics, Chinese Academy of Sciences, Lanzhou, 730000, China

ABSTRACT

Water oxidation reaction is the bottleneck process of water splitting. The exploration of efficient water oxidation catalysts (WOCs) is of great importance for accelerating this reaction. Herein, a cobalt(II)-containing complex $\{K_2[CoO_3PCH_2N(CH_2CO_2)_2]\}_6$ (K_{12}**1**) with symmetrical hexameric ring structure and polynuclearity as an efficient visible light-driven WOC is reported. Using $[Ru(bpy)_3](ClO_4)_2$ as photosensitizer and $Na_2S_2O_8$ as sacrificial electron acceptor, an optimal oxygen yield of 62.6%, turnover number (TON) of 4350 and turnover frequency (TOF) of 162.6 s^{-1} are obtained. To the best of our knowledge, this TON and TOF are the highest value among all the catalyst for light driven water oxidation. In addition, a high quantum yield of 60.6% is achieved. Investigation including UV–vis absorption, infrared (IR) spectroscopy, X-ray photoelectron spectroscopy and other techniques confirm that **1** is a stable and efficient catalyst for visible light-driven water oxidation. Collective experiments demonstrate that **1** catalyses visible light-driven water oxidation via water nucleophilic attack (WNA) process and its high activity may be originated from the multiple sites water oxidation catalysis.

1. Introduction

Climate change and environmental pollution caused by the excessive use of fossil fuels and the increasing energy demand of mankind have attracted much attention in recent years [1,2]. Development of renewable clean energy such as hydrogen is considered to be a feasible solution to resolve these problems [3,4]. Light-driven water splitting inspired by photosynthesis system II (PSII) has the potential of transforming solar energy and abundant water resource into hydrogen energy [5]. The splitting of water is a process involved in four electrons and four protons. It contains two half reactions: oxidation of water ($2H_2O \rightarrow 4H^+ + O_2 + 4e^-$) and reduction of remained protons ($4H^+ + 4e^- \rightarrow 2H_2$) [6,7]. Water oxidation step with high activation energy is regarded as the bottleneck process for overall water splitting. The searching of efficient water oxidation catalysts (WOCs) is very meaningful and challenging [8].

Heterogeneous light-driven WOCs such as metal oxides or bimetal oxides [9–13], metal sulfides [14] and metal phosphates [15,16] have been extensively researched. Compared with these heterogeneous WOCs, homogeneous WOCs, especially the organic ligand based complexes have more advantages with structure modification and mechanistic understanding [17]. Since the "blue dimmer" was reported by Meyer as the first example of homogenous catalyst for water oxidation in 1982 [18], plenty of homogeneous WOCs containing Ru or Ir have been documented [19–23]. Considering the low cost and abundance factor, increasing attentions have been paid to the development WOCs based on the first-row abundant transition metal [24–29]. Among which cobalt based homogeneous molecular catalysts are very attractive because most of them have shown excellent water oxidation activity [30,31]. Compared with all-inorganic coordination compounds such as polyoxometalates as WOCs [32–34], the usage of complex containing organic ligand as homogeneous WOCs is more critical and challenging in view of oxidative instability of the ligand [35,36]. Besides the oxidative stability, the hydrolytic stability and the purity of the molecular organic complex catalysts are also the research focus for WOCs. Some molecular cobalt organic complexes catalyzed the visible light-driven water oxidation by decomposing itself into heterogeneous active species such as CoO_x during the reaction [36,37]. On the other hand, some molecular cobalt-containing complexes turn out to be inactive and the true catalytic capability originates from Co(II) impurities introduced from their synthetic process [38,39]. Therefore, sufficient experimental evidences should be provided to identify a homogeneous

molecular WOC.

On the other hand, many robust, molecular complexes with polynuclear structure have been developed as WOC in recent years. These complexes usually own excellent catalytic activity, whether in photochemical or electrochemical water oxidation system [40–45]. Some dinuclear and polynuclear homogeneous WOCs catalyze water oxidation via intramolecular O−O bond formation and afford outstanding catalytic activity [44–46]. The polynuclear structures of these WOCs provide a convenient pathway for intramolecular O−O bond formation. In another case, some polynuclear complexes own multiple water-binding sites or multiple unsaturated coordination sites, which offer the possibility of homogeneous electrochemical and chemical water oxidation catalysis at multiple sites. The independent catalytic process taking place at multiple sites affords their high catalytic activity for water oxidation [22,47].

Inspired by those works, we believe that some polynuclear molecular homogeneous WOCs may accelerate visible light-driven oxygen evolution via efficient water oxidation catalysis taking place on multiple sites that do not interfere with each other. In this work, we describe the synthesis and water oxidation performance of a hexameric ring cobalt-containing macrocycle $[Co(PMIDA)]_6^{12-}$ (**1**, H_4PMIDA = N-(Phosphonomethyl)-iminodiacetic acid, Fig. 1). This macrocyclic architecture is composed of six self-same $[Co(PMIDA)]^{2-}$ monomer and it is capable of catalyzing visible light-driven water oxidation with unprecedented efficiency. Optimal oxygen yield, TON and TOF of 62.6%, 4350 and 162.6 s^{-1} are obtained using $[Ru(bpy)_3]$ $(ClO_4)_2$ as photosensitizer and $Na_2S_2O_8$ as sacrificial electron acceptor in borate buffer solution. It should be noted that a high quantum yield of 60.6% is achieved. Of the reported catalysts for visible light-driven water oxidation, **1** affords the highest TON and TOF. Collective experiments demonstrate that **1** is a homogeneous WOC. It catalyses visible light-driven water oxidation via water nucleophilic attack (WNA) process and its high activity may be originated from the multiple sites water oxidation catalysis.

2. Experiment section

2.1. Material

Purified water (18.2 MΩ cm, TOC < 3 ppb) used for preparing solutions was produced by Molecular Lab Water Purifier, and all other chemicals and salts used were of the highest purity available from commercial sources.

2.2. Catalyst preparation

K_{12}**1** was synthesized by hydrothermal method according to a previous literature [48] with some modifications. A solution of Co $(OAc)_2 \cdot 4H_2O$ (0.375 g, 1.5 mmol) in methanol (2 mL) was added to a stirred solution of methanol (8 mL) containing $H_2O_3PCH_2N$ $(CH_2CO_2H)_2 \cdot H_2O$ (0.367 g, 1.5 mmol) and KOH (0.337 g, 6 mmol). The blue slurry obtained by simply stirring was put into a Teflon liner stainless steel autoclave with 23 mL capacity. The autoclave was kept at 200 °C for 48 h and cooled to room temperature slowly. Blue-purple hexagonal crystals were formed and collected by filtration. It was washed several times with methanol and dried at ambient temperature. TG analysis in nitrogen atmosphere indicates the existence of 2.5 lattice water in the molecular structure (Fig. S1). Elemental analysis calculated (%) for $C_{30}H_{36}N_6O_{42}Co_6K_{12}P_6 \cdot 2.5H_2O$: Co 16.36, K 21.70, P 8.61, C 16.65, H 1.67 and N 3.87; Found: Co 16.82, K 21.36, P 8.89, C 17.13, H 1.93 and N 3.69. The valence of Co element in K_{12}**1** as synthesized was verified by XPS measurements. In the high resolution XPS spectrum, the binding energy of Co is corrected by C 1 s peak (284.8 eV) (Fig. S2). Two peaks observed at 780.5 eV and 796.5 eV with two satellite peaks at 785.5 eV and 801.5 eV are assigned to Co $2P_{3/2}$ and Co $2P_{1/2}$, respectively, which are the characteristic peak of Co(II). The XPS result demonstrates that the valence of Co element in K_{12}**1** as prepared is +2.

3. Results and discussion

3.1. Crystallography of catalyst

X-ray structure analysis shows that the structure of **1** in this compound is formed by six simple structural units in which each of the cobalt (II) ions is five-coordinated with geometry of distorted trigonal bipyramid (Fig. 1). The nitrogen atom provided by the ligand N-Phosphonomethyl)iminodiacetic acid lies at one apex and the three arms of the ligand coordinate equatorially. This unit is the monomer from which hexameric rings are formed. A phosphonate oxygen atom from a neighboring monomer occupies the other apical coordination site of the cobalt(II) ion, such that the oligomers with head-tail closed loop model are formed. The good similarity between powder X-ray diffraction (PXRD) pattern of K_{12}**1** and that from single-crystal X-ray diffraction indicates its high phase purity (Fig. 2).
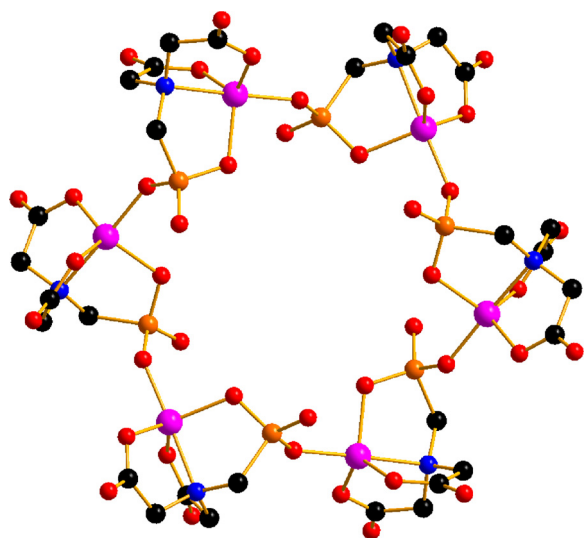

Fig. 1. Ball-and-stick representation of **1**, (Co, pink; P, orange; O, red; C, black; N, blue; H atoms and counter cations were omitted for clarity). (For interpretation of the references to colour in this figure legend, the reader is referred to the web version of this article).
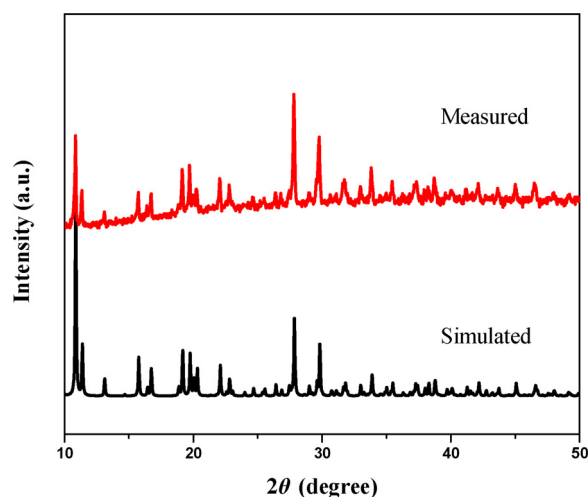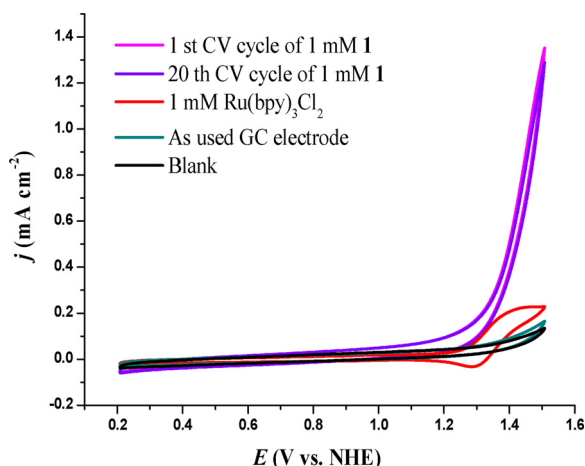

Fig. 2. PXRD patterns of K_{12}**1**: simulated data (black) and measured data (red). (For interpretation of the references to colour in this figure legend, the reader is referred to the web version of this article).

Fig. 3. Cyclic voltammetry of 1, photosensitizer $Ru(bpy)_3^{2+}$ and the as used GC electrode in 80 mM borate buffer at pH 9.0. The blank line displays the CV of the no-catalyst buffer solution. A glassy carbon (GC) electrode (active area = 0.071 cm^2), Ag/AgCl (3.5 M KCl) and Pt wire electrode as the working, reference and auxiliary electrodes, respectively, the scan rate is 100 mV/s.

3.2. Electrochemical measurements

CV measurements were carried out to test the electrochemical properties of **1**. As shown in Fig. 3, no obvious redox wave can be observed when **1** was characterized by cyclic voltammetry. The onset potential of the water oxidation at pH 9.0 catalyzed by **1** is 1.32 V vs. NHE (pink trace). The maximal catalytic current at 1.45 V vs. NHE is 1.35 mA cm^{-2}. The controlled experiment for comparison was conducted by testing the borate buffer without **1**. A negligible catalytic current (black trace) is obtained under this condition, which confirms **1** indeed catalyzes the water oxidation reaction. After 20 scan cycles of **1** in borate buffer, the catalytic current remains unchanged (purple trace). In addition, after the 20 scan cycles, the as used GC electrode was washed with pure water without polishing. It was tested by the cyclic voltammetry in fresh borate buffer (pH 9.0) and ignored catalytic current was observed (cyan trace). The above experiments illustrate four facts as follows: Firstly, there is no active cobalt species deposited on the surface of GC electrode; secondly, no Co(II) impurities exist in the as synthesized catalyst; thirdly, **1** keeps the chemical structure under the experimental condition; fourthly, **1** is oxidative stable and is capable of acting as a homogeneous molecular WOC. Meanwhile, the cyclic voltammetry of the photosensitizer $[Ru(bpy)_3]Cl_2$ was conducted (red trace). The measured redox potential of $Ru(bpy)_3^{3+/2+}$ is 1.37 V vs. NHE (Fig. S4). Therefore, $Ru(bpy)_3^{3+}$ is thermodynamically capable of driven water oxidation with **1**.

3.3. Photocatalytic water oxidation

The optimum reaction conditions for water oxidation were obtained through varying the catalyst concentrations, photosensitizer concentrations, sacrificial electron acceptor concentrations, light intensity and pH value of the reaction solution (Fig. 4a and Figs. S5–S8). **1** showed no activity in the absence of photosensitizer $[Ru(bpy)_3]^{2+}$, or sacrificial electron acceptor $Na_2S_2O_8$ or light irradiation. Therefore, photosensitizer, sacrificial electron acceptor and light irradiation are indispensable conditions to the visible light-driven water oxidation (Fig. S9). Nearly no oxygen was detected in the absence of **1**, indicating that **1** indeed acts the role of catalyst and accelerates the oxidation of water. When **1** was added, oxygen was formed very quickly and O_2 evolution achieved to a plateau after around 150 s because of the consumption of $Na_2S_2O_8$ and photosensitizer (Fig. 4a). Continuous increase of concentrations of **1** from 0.1 μM to 7.0 μM leads to the increase of oxygen yield, while higher catalyst concentration (9.0 μM)
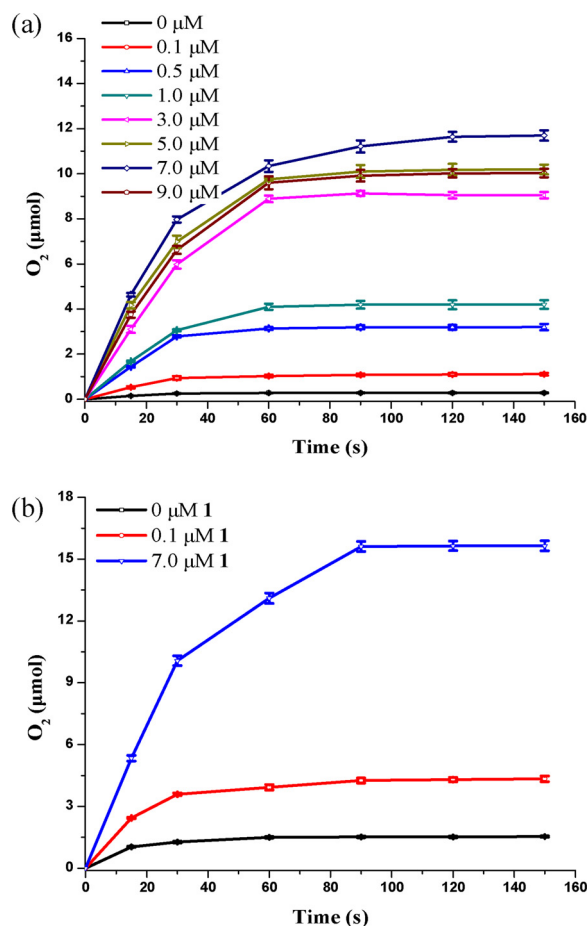
Fig. 4. (a) Plots of oxygen evolution catalyzed by various concentrations of **1** in 10 mL 80 mM borate buffer solution (pH 9.0, 23 °C) containing 1 mM [Ru (bpy)$_3$]Cl$_2$ and 5 mM Na$_2$S$_2$O$_8$. (b) Plots of oxygen evolution catalyzed by various concentrations of **1** in 10 mL 80 mM borate buffer solution (pH 9.0, 23 °C) containing 1 mM [Ru(bpy)$_3$](ClO$_4$)$_2$ and 5 mM Na$_2$S$_2$O$_8$. All reaction systems were irradiated by LEDs (λ = 460 nm, 33.8 mW cm^{-2}).

lowers the oxygen yield. The optimal yield of oxygen was 46.8%. The optimal TON of 1125 and TOF of 35.3 s^{-1} were obtained over 0.1 μM of **1**, demonstrating outstanding catalytic activity of **1** in comparison with others WOCs under light driven water oxidation system (Tables 1 and S2 and S3, Figs. S10–S13). Replacing $[Ru(bpy)_3]Cl_2$ by $[Ru(bpy)_3]$ $(ClO_4)_2$, **1** exhibited unprecedented activity for catalyzing water oxidation (Figs. 4b and S14) with an optimal oxygen yield, TON and TOF of 62.6%, 4350 and 162.6 s^{-1}, respectively. To the best of our knowledge, the TON and TOF are the highest values among all the light driven water oxidation reaction system. The quantum yield and O_2 yield are also above averages of other WOCs (Tables 1, S2). The reaction mechanism of the visible light-driven water oxidation catalyzed by **1** is depicted in Scheme 1.

The role of **1** in this reaction was further investigated by measuring the UV–vis absorption spectrum of the borate buffer solution containing 1 mM $[Ru(bpy)_3]Cl_2$ and 5 mM $Na_2S_2O_8$. A characteristic absorption peak at 450 nm (Fig. S15, black trace) is attributed to the absorption of $[Ru(bpy)_3]Cl_2$. When the reaction system was irradiated for 150 s by LEDs, the characteristic absorption of the reaction solution at 450 nm showed a decrease of 23.7% (blue trace), which was ascribed to the decomposition of photosensitizer. However, a decrease of only 10.1% was observed when a reaction solution containing 7.0 μM **1** was irradiated (red trace). Therefore, **1** can reduce the decomposition of photosensitizer.

In order to confirm that water oxidation reaction is not dependent

Table 1
Photocatalytic activity of various homogeneous WOCs in Ru(bpy)$_3^{2+}$/Na$_2$S$_2$O$_8$ system.

Catalyst material	TON[a]	TOF (s^{-1})[b]	Φ_{QY} (%)[c]	O$_2$ yield (%)[d]	Refs.
1	1125	35.3	5.9	4.5	This work[e]
1	4350	162.6	27.1	17.4	This work[f]
1	223	5.2	60.6	62.6	This work[f]
[Co$_4$(H$_2$O)$_2$(PW$_9$O$_{34}$)$_2$]$^{10-}$	224	No data	30	45	[49]
[Co$_4$(hmp)$_4$(μ-OAc)$_2$-(μ_2-OAc)$_2$(H$_2$O)$_2$]	40	7	No data	32	[30]
[Mn$_4$V$_4$O$_{17}$(OAc)$_3$]$^{3-}$	1150	1.75	No data	7.2	[42]
[Fe$_{11}$(H$_2$O)$_{14}$(OH)$_2$-(W$_3$O$_{10}$)$_2$(α-SbW$_9$O$_{33}$)$_6$]$^{27-}$	1815	6.3	47	94	[28]
[{β-SiNi$_2$W$_{10}$O^{36-}(OH)$_2$(H$_2$O)}$_4$]$^{24-}$	335	1.7	17	13.3	[50]
[Ru(bda)bpb]$_3$	1255	13.1	NO data	< 1	[22]
[{Ru$_4$O$_4$(OH)$_2$(H$_2$O)$_4$}-(γ-SiW$_{10}$O$_{36}$)$_2$]$^{10-}$	180	0.08	26	38	[51]
PSII-WOC[g]	10^7	500	No data	No data	[40]

[a] TON is defined as total number of mole of O$_2$ / mole of catalyst.
[b] TOF = TON/Time.
[c] Φ_{QY} (%, quantum yield) = 2 × initial O$_2$ formation rate/photon flux.
[d] O$_2$ Yield = 2 × mole of O$_2$ per mole of Na$_2$S$_2$O$_8$.
[e] [Ru(bpy)$_3$]Cl$_2$ as photosensitizer.
[f] [Ru(bpy)$_3$](ClO$_4$)$_2$ as photosensitizer.
[g] P680 chlorophylls and Tyr radical as photosensitizer and sacrificial electron acceptor, respectively.
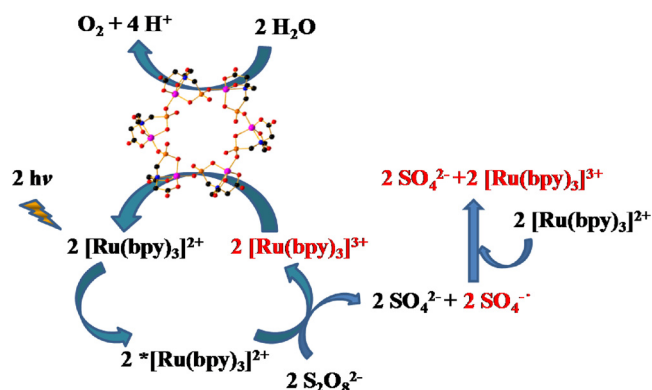
Scheme 1. Principal processes of an O$_2$ evolution light-driven water oxidation system.

on the persulfate and sulfate radical formed during the reaction. Chemical prepared [Ru(bpy)$_3$](ClO$_4$)$_3$ was used as oxidant to conduct chemical water oxidation at pH 9.0. When 7.0 μM **1** was used as catalyst, the increased evolution of oxygen took place with the increase of concentration of [Ru(bpy)$_3$](ClO$_4$)$_3$ (Fig. S16). As mentioned above, Na$_2$S$_2$O$_8$ is incapable of oxidizing water without assistance of **1** and [Ru(bpy)$_3$]$^{2+}$. Therefore, **1** was oxidized to high valence species by photogenerated [Ru(bpy)$_3$](ClO$_4$)$_3$ rather than Na$_2$S$_2$O$_8$. When the visible light driven water oxidation was conducted at pH 8.0, [Ru(bpy)$_3$]$^{3+}$ can be detected in the reaction system without addition of **1** (Fig. S17, the characteristic absorption at 670 nm is assigned to [Ru(bpy)$_3$]$^{3+}$ [52]). In contrast, when **1** was used a catalyst, [Ru(bpy)$_3$]$^{3+}$ can not be detected, further confirming that **1** can react with photo-generated [Ru(bpy)$_3$]$^{3+}$. Nanosecond laser flash photolysis experiments (Fig. 5) were further conducted to investigate the catalytic capability of **1** during the process of light-driven water oxidation. The [Ru(bpy)$_3$]$^{2+}$ was oxidized to [Ru(bpy)$_3$]$^{3+}$ by Na$_2$S$_2$O$_8$ in a few microseconds after irradiation.
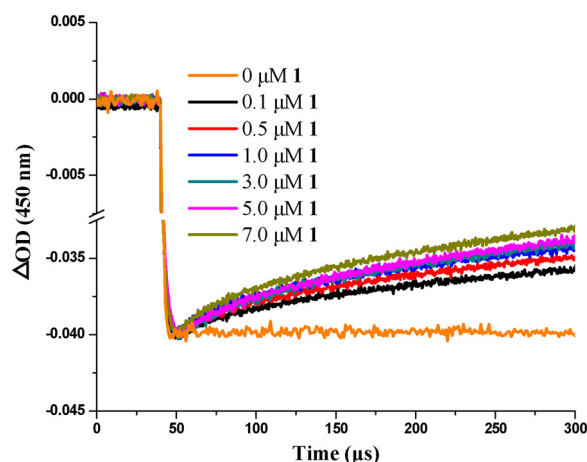
Fig. 5. [Ru(bpy)$_3$]$^{3+}$-scavenging kinetics measured using different concentration of **1**. Kinetics of the bleach recovery were collected under the following experimental conditions: excitation wavelength = 445 nm; analysis wavelength = 450 nm; 50 μM [Ru(bpy)$_3$]Cl$_2$ and 5 mM Na$_2$S$_2$O$_8$ in 80 mM sodium borate buffer (pH = 9.0).

The orange curve corresponds to the constant concentration of in situ generated [Ru(bpy)$_3$]$^{3+}$ in the absence of **1**. Other curves with decreased ΔOD trend correspond to different quenching rates of [Ru(bpy)$_3$]$^{3+}$, verifying the [Ru(bpy)$_3$]$^{3+}$-scavenging activity of **1** (i.e. oxidation of **1** by [Ru(bpy)$_3$]$^{3+}$). With the concentration of **1** increasing, the [Ru(bpy)$_3$]$^{3+}$-scavenging activity of **1** increases accordingly. Therefore, the light-driven water oxidation reaction occurs via the oxidation of **1** to high valence, which is similar to Mn$_4$CaO$_5$ cluster in PS II [5].

3.4. Verification of catalyst stability

In view of activity or kinetics, **1** is absolutely different from simple Co^{2+}. On the one hand, **1** exhibits higher activity compared with Co^{2+} under identical condition (Fig. S18). On the other hand, for the visible light-driven water oxidation system, the precatalysts whose catalytic activity originates from CoO$_x$ produced by autolysis or hydrolysis, always show a large lag phase compared with those true homogeneous catalysts [36]. Fig. S18 illustrates the plots of water oxidation catalyzed by Co(OAc)$_2$·4H$_2$O and **1**. As expected, Co(OAc)$_2$·4H$_2$O exhibits a lag phase within the first 30 s, while **1** does not show any lag phase. Therefore, the catalytic properties of **1** are obviously different from that of the documented precatalyst of Co^{2+} ions for visible light-driven water oxidation. **1** does not decompose into CoO$_x$ during water oxidation. Furthermore, during the reuse experiment, 7.0 μM **1** after a standard test was added fresh Na$_2$S$_2$O$_8$ and the pH value of the post reaction solution was readjusted to 9.0. Oxygen yield of 66%, 51% and 28% were achieved in the first, second and third recycling test, respectively (Fig. S19 and S20). For direct comparison, the corresponding amount of Co^{2+} was used as WOC, showing a more pronounced decrease of catalytic activity in the second, third recycling test. The recycling activity tests of **1** by adding [Ru(bpy)$_3$]Cl$_2$ and Na$_2$S$_2$O$_8$ were also conducted, a relatively low activity decrease was observed after each recycling test when both [Ru(bpy)$_3$]Cl$_2$ and Na$_2$S$_2$O$_8$ were added, indicating that the loss of recycling catalytic activity is due to photosensitizer decomposition (Fig. S21) [30]. On the other hand, after illumination, Clark electrode kinetics of **1** show a lag phase of 2–3 s before oxygen evolution started (Fig. 6). The small lag phase is attributed to the accumulation of [Ru(bpy)$_3$]$^{3+}$ to drive water oxidation.

Genuine homogeneous catalytic essence of **1** was further confirmed by chelation experiment. To further rule out such a possibility that the catalytic activity of **1** originates from Co^{2+} ions impurities, ethylenediamine tetraacetic acid (EDTA) was added to the reaction solution. As
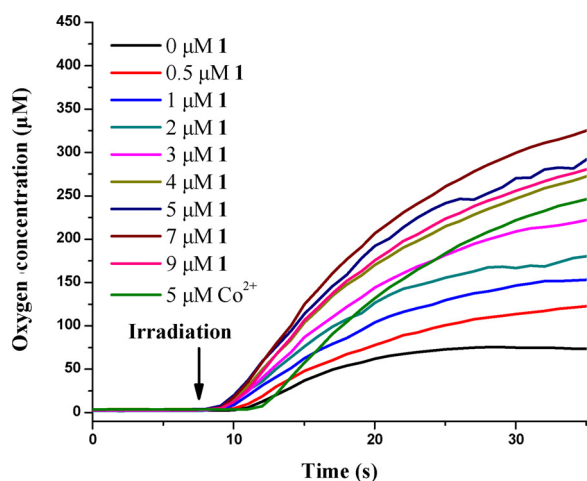
Fig. 6. Plots of O_2 evolution catalyzed by $Co(OAc)_2 \cdot 4H_2O$ and **1** at various concentrations in 10 mL 80 mM borate buffer solution (pH 9.0) containing 1 mM $Ru(bpy)_3Cl_2$ and 5 mM $Na_2S_2O_8$. This reaction systems were irradiated using LEDs (λ = 460 nm, 33.8 mW cm^{-2}), the arrow indicates the start of the irradiation.
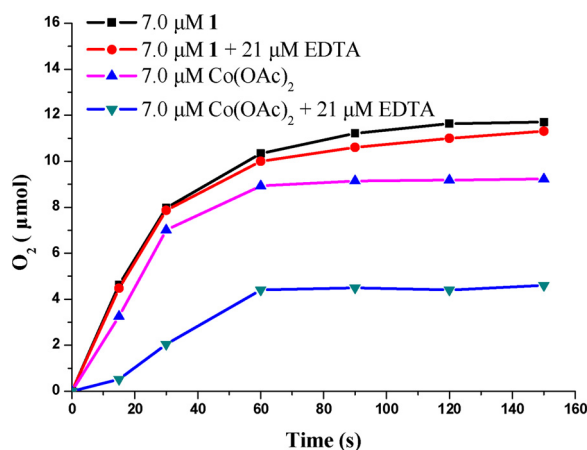
Fig. 7. Plots of oxygen evolution vs. time for catalytic water oxidation in 10 mL 80 mM borate buffer solution (pH 9.0) containing 7.0 μM **1**, 1 mM $Ru(bpy)_3Cl_2$ and 5 mM $Na_2S_2O_8$. Effects of the concentration of chelating agent EDTA: (blank) 0 μM, (red) 21 μM, all reaction systems were irradiated using LEDs (λ = 460 nm, 33.8 mW cm^{-2}). (For interpretation of the references to colour in this figure legend, the reader is referred to the web version of this article).

shown in Fig. 7, the plot of oxygen evolution vs. time remains nearly unchanged when 3 eq. EDTA (21 μM) is added to the reaction solution, revealing that there is no Co(II) impurities existence in **1**. Since Co(II) impurities are easily to be completely chelated by a small amount of chelating agent, e.g., EDTA or bipyridine and the oxygen evolution will completely stop if **1** contains the impurities. Here, for catalyst **1**, the addition of EDTA has no effect on the water oxidation, indicating that the catalytic activity of catalyst as synthesized is really originated from **1** instead of impurities containing cobalt. From this point, **1** gives the characteristic of genuine homogeneous molecular WOC. Plots of oxygen evolution vs. time catalyzed by **1** aged 3 h and fresh **1** are almost the same (Fig. S22), confirming that **1** keeps the chemical structure in borate buffer solution during aging treatment and shows no decay of activity.

Addition of acetone to the post-reaction solution led to the precipitate containing **1**. This suspension was centrifuged and the precipitate was washed with acetone and then dried at ambient temperature. Elemental analysis (Table S4) of this precipitates shows that the molar ratio of Co element and P element in this precipitate remains
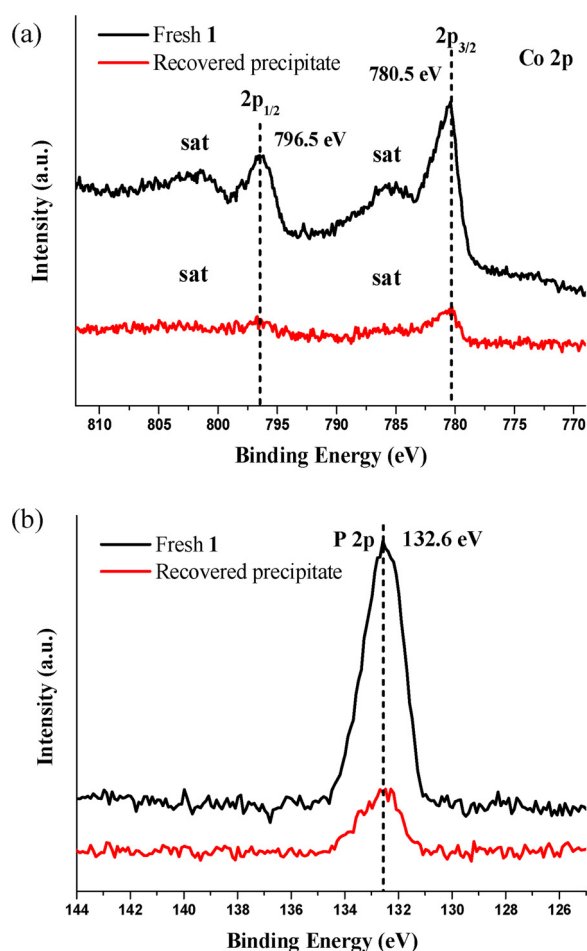

Fig. 8. XPS spectra of (a) Co 2p and (b) P 2p of pristine **1** and recovered precipitate, respectively.

constant compared with that of the fresh **1**, revealing that **1** in this precipitate is intact. The fresh catalyst and recovered precipitate were further characterized by IR spectroscopy, as shown in Fig. S23 and S24, the IR spectrum of the recovered precipitate remains all the characteristic peaks of the fresh **1**, confirming the structural integrity **1** during water oxidation. Herein, the XPS characterization was applied to identify the durability of metal complex. XPS full scans of the samples are shown in Fig. S25. Compared with the fresh **1**, the XPS spectrum of precipitate presents additional characteristic peaks of Na and Ru element, which is resulted from the precipitated sodium borate (or $Na_2S_2O_8$) and photosensitizer. Most of all, the peak intensities of Co 2p and P 2p decrease to the same extent (the recovered **1** is only a part of this precipitate), and the binding energy values of those keep invariable (Fig. 8), indicating that the chemical environments of Co and P in the recovered catalyst are the same as the pristine **1**. In all, elemental analysis, IR and XPS characterizations together demonstrate that the structure of **1** keeps integrity before and after water oxidation reaction.

4. Mechanism investigation

Clarification of mechanistic of the water oxidation process is significant because it gives intelligent guidance to design new efficient WOCs. Whether **1** operates water oxidation catalysis via the WNA process or interaction of two metal oxide units (I2M) mechanism pathway should be clarified. Obviously, suitable distance between two adjacent nuclear is critical for the intermolecular O–O bond formation (No matter through multiple active sites cooperation or interaction of two metal oxide units). Just as the pentanuclear iron catalyst
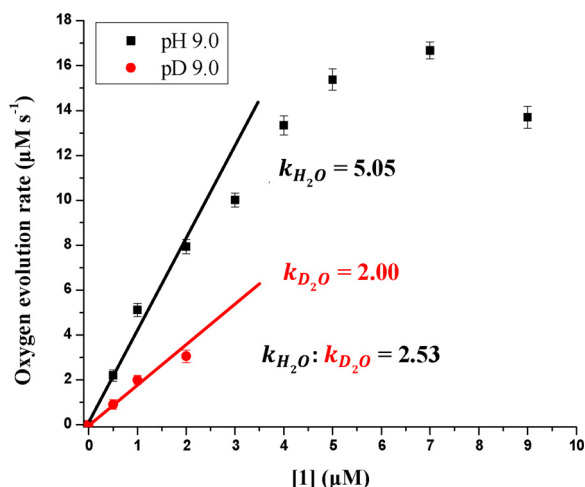
Fig. 9. Plots of initial rate of O_2 evolution vs. the concentration of **1** in H_2O and D_2O in 80 mM borate buffer solution (pH 9.0 and pD 9.0, 23 °C) containing 1 mM [Ru(bpy)$_3$]Cl$_2$ and 5 mM Na$_2$S$_2$O$_8$. This reaction system was irradiated using LEDs (λ = 460 nm, 33.8 mW cm^{-2}).

[Fe$_4^{II}$Fe^{III}(μ_3-O)(μ-L)$_6$]$^{3+}$ (LH = 3,5-bis(2-pyridyl)pyrazole), in which the O−O bond is formed between two most adjacent Fe^{III} ions during water oxidation process [44]. Co based homogeneous WOCs have been found to catalyze oxygen evolution via I2M process mechanism pathway and intramolecular O−O bond formation between two adjacent Co cores [46,53]. {Co^{III}(μ_2-O$_2$)(μ_2-OH)Co^{III}} intermediate in

catalytic cycle was formed from {Co^{III}(μ_2-OH)Co^{III}} fragments in [Co$_2^{III}$(μ-OH)$_2$(TPA)$_2$]$^{4+}$ (TPA = tris(2-pyridylmethyl)amine), in which the distance between two Co ions is shorter than 3.0 Å [46]. The [Co^{III}]$_2$(μ-OOH) intermediate has been proven in water oxidation catalysis by [Co$_2$(μ-OH)$_2$(OH$_2$)$_2$(DPFN)]$^{4+}$ (DPFN = 2,7-bis(fluoro -di(2-pyridyl)methyl)-1,8-naphthyridine), which fixes two Co^{III} ions with a distance of 2.783 Å by DPFN ligand and acts as a molecular structural analog of proposed active sites of cobalt phosphate water oxidation catalysts [53]. Meanwhile, the distance between two Co ions bridged by μ-O$_2$ in some kinetically stable dicobalt, dioxygen adducts is shorter than 3.9 Å [39,54]. However, the distance of adjacent Co ions in **1** is 5.5 Å, which is too long for the formation of bridge O−O bond (Table S5). Therefore, the intramolecular O−O bond formation between adjacent Co ions in **1** is infeasible.

We investigated the redox property of [Co(PMIDA)]$^{2-}$ center in **1** by differential pulse voltammetry (DPV) experiment (Fig. S26). E$_{1/2}$ values for the redox processes studied in this work are estimated according to the potential at the maximal current in DPV measurements. Only one oxidation process is observed, the potential of which is pH-dependent and variable in the range between 1.30–1.48 V vs. NHE with a slope of − 62 mV/pH unit (Fig. S27). The redox couple of [L-Co^{III}]/[L-Co^{II}] (L = ligand) is commonly reported to be below 1.0 V vs NHE at pH 9.0. However, no redox wave is observed when the CV measurement of **1** is conducted in low potential. (Fig. S28). Therefore, the potential range between 1.30–1.48 V vs. NHE should be assigned to the oxidation of Co(III) to Co(IV), and it is a proton-coupled electron transfer (PCET) process of –H$^+$/-e-.

The initial reaction rate is relevant to the catalyst concentration of **1**. When the concentration of **1** is lower than 2.0 μM, initial rates of the
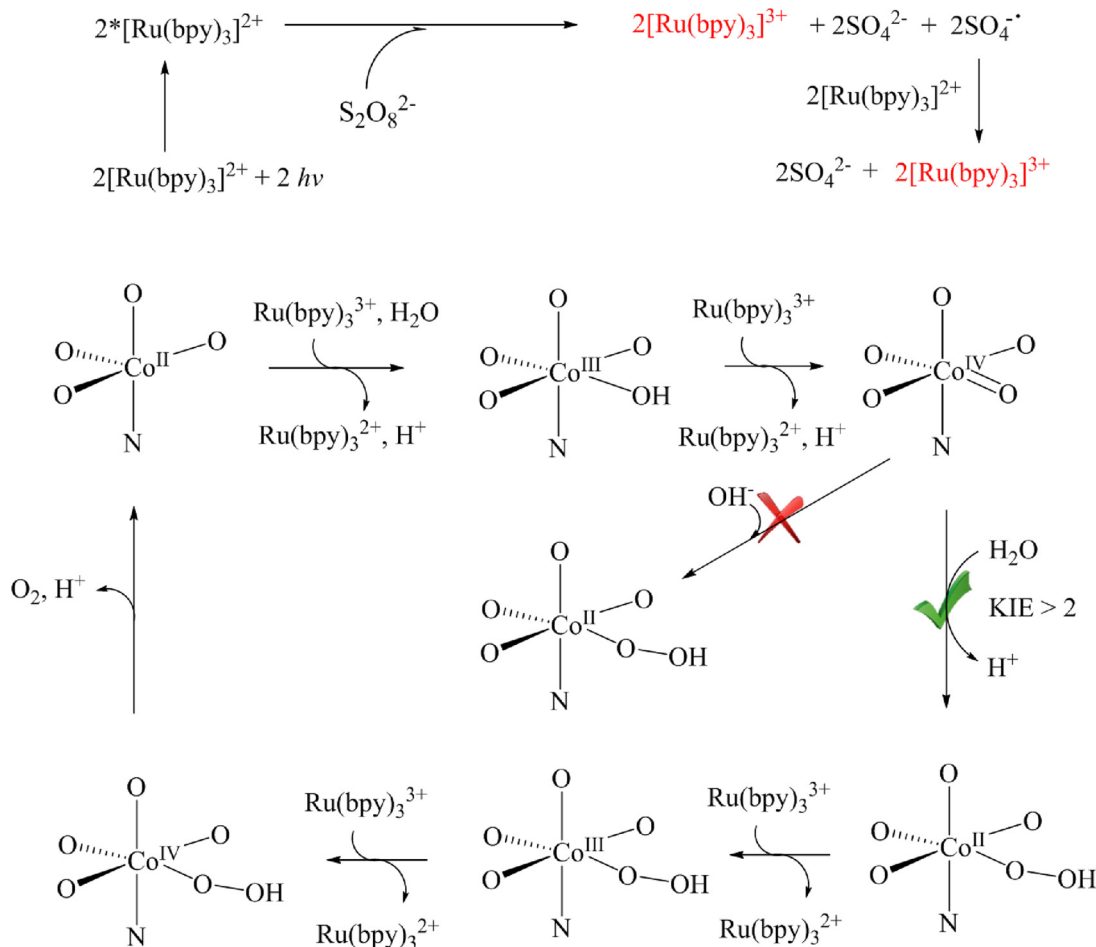
Scheme 2. Proposed mechanism of visible light-driven water oxidation reaction catalysed by **1**.

oxygen evolution depends linearly on the concentration of **1**, giving a first-order rate constant of $k = 5.05$ s^{-1} (Figs. 6 and 9). However, the initial rate of water oxidation levels off and then reduces when **1** with high concentration is used. This first-order relation between the initial rates and the low concentrations of catalyst is a distinct feature of homogeneous catalytic system [55,56]. Proton coupled process is often reported to be involved in the rate-determining step (RDS) of water oxidation. To verify whether the RDS of the water oxidation reaction process in this work is a proton coupled process, the rate of water oxidation catalyzed by **1** was measured in D$_2$O buffer solution (Fig. S29). Direct O−H/D bond breaking during the RDS of the catalytic process will lead to kinetic isotope effect (KIE), which differ by a factor at least 2 in H$_2$O and D$_2$O [22,57]. By quantifying the initial rates using different concentrations of **1**, the reaction velocities in D$_2$O were obtained. The plot of initial rate versus catalyst concentration of **1** in D$_2$O gives an initial rate constant of 2.00 s^{-1} (Fig. 9). Therefore, a KIE value of 2.53 ((k_{H_2O}/k_{D_2O}) is obtained, providing solid evidence for the proton coupled process in the RDS. KIE result has also been used to distinguish WNA ($k_{H_2O}/k_{D_2O} > 2$) and I2M process in water oxidation. Fig. 9 indicates that oxygen-oxygen bond is formed via WNA process rather than interaction of two metal oxide units and an O−H bond breaking process is involved in the formation of Co(II)-hydroperoxide species.

Based on the experimental data, the following mechanism for water oxidation catalyzed by **1** is proposed (Scheme 2). Firstly, Co(IV)-oxo intermediate is supposed to be generated by two consecutive one-electron oxidation of **1** by Ru(bpy)$_3$$^{3+}$ under irradiation conditions. Secondly, the Co(IV)-oxo species converts to peroxide species Co(II)-hydroperoxide through water molecular nucleophilic attack accompanied by intramolecular charge transfer rather than hydroxyl nucleophilic attack. Thirdly, the Co(II)-hydroperoxide species will be further oxidized by Ru(bpy)$_3$$^{3+}$ to produce Co(IV)-hydroperoxide. Finally, O$_2$ is released by intramolecular charge transfer of Co(IV)-hydroperoxide species.

5. Conclusion

In summary, a hexameric ring complex {K$_2$[CoO$_3$PCH$_2$N (CH$_2$CO$_2$)$_2$]}$_6$ (K$_{12}$**1**) is confirmed as a genuine homogeneous efficient WOC by collective experimental techniques. The catalytic mechanism was proposed according to electrochemical and photochemical characterization techniques. Systematic research reveals Co nuclear in **1** can function as active site independently during water oxidation. The high efficiency of oxygen evolution may be due to water oxidation catalysis taking place at multiple sites on the **1** molecular. Constructing molecular complex with dinuclear or tetranuclear cubane-like structure that facilitates I2M has been regarded as a method to develop efficient WOCs. Based on our research on **1**, developing polynuclear molecule WOCs with multiple active sites that can work independently to form O−O bond during catalytic process is supposed to be a new strategy to achieve highly efficient water oxidation catalysts.

Acknowledgements

Appendix A. Supplementary data

Supplementary material related to this article can be found, in the online version, at doi: https://doi.org/10.1016/j.apcatb.2018.09.052.

References

[1] N.S. Lewis, D.G. Nocera, Proc. Natl. Acad. Sci. U. S. A. 103 (2006) 15729–15735.
[2] D.G. Nocera, Chem. Soc. Rev. 38 (2009) 13–15.
[3] D. Gust, T.A. Moore, A.L. Moore, Acc. Chem. Res. 42 (2009) 1890–1898.
[4] H.B. Gray, Nat. Chem. 1 (2009) 7-7.
[5] M.D. Kärkäs, O. Verho, E.V. Johnston, B. Åkermark, Chem. Rev. 114 (2014) 11863–12001.
[6] S. Romain, L. Vigara, A. Llobet, Acc. Chem. Res. 42 (2009) 1944–1953.
[7] L. Duan, L. Wang, F. Li, F. Li, L. Sun, Acc. Chem. Res. 48 (2015) 2084–2096.
[8] J.D. Blakemore, R.H. Crabtree, G.W. Brudvig, Chem. Rev. 115 (2015) 12974–13005.
[9] D. Hong, Y. Yamada, T. Nagatomi, Y. Takai, S. Fukuzumi, J. Am. Chem. Soc. 134 (2012) 19572–19575.
[10] J. Rosen, G.S. Hutchings, F. Jiao, J. Am. Chem. Soc. 135 (2013) 4516–4521.
[11] G. Chen, L. Chen, S.-M. Ng, W.-L. Man, T.-C. Lau, Angew. Chem. Int. Ed. 52 (2013) 1789–1791.
[12] D.M. Robinson, Y.B. Go, M. Mui, G. Gardner, Z. Zhang, D. Mastrogiovanni, E. Garfunkel, J. Li, M. Greenblatt, G.C. Dismukes, J. Am. Chem. Soc. 135 (2013) 3494–3501.
[13] Y. Zhang, J. Huang, Y. Ding, Appl. Catal. B-Environ. 198 (2016) 447–456.
[14] M. Zheng, Y. Ding, L. Yu, X. Du, Y. Zhao, Adv. Funct. Mater. 27 (2017) 1605846.
[15] T. Zhou, D. Wang, S. Chun-Kiat Goh, J. Hong, J. Han, J. Mao, R. Xu, Energy Environ. Sci. 8 (2015) 526–534.
[16] Q. Xu, H. Li, L. Chi, L. Zhang, Z. Wan, Y. Ding, J. Wang, Appl. Catal. B-Environ. 202 (2017) 397–403.
[17] L. Duan, L. Tong, Y. Xu, L. Sun, Energy Environ. Sci. 4 (2011) 3296–3313.
[18] S.W. Gersten, G.J. Samuels, T.J. Meyer, J. Am. Chem. Soc. 104 (1982) 4029–4030.
[19] N.D. McDaniel, F.J. Coughlin, L.L. Tinker, S. Bernhard, J. Am. Chem. Soc. 130 (2008) 210–217.
[20] L. Duan, F. Bozoglian, S. Mandal, B. Stewart, T. Privalov, A. Llobet, L. Sun, Nat. Chem. 4 (2012) 418–423.
[21] J.M. Thomsen, S.W. Sheehan, S.M. Hashmi, J. Campos, U. Hintermair, R.H. Crabtree, G.W. Brudvig, J. Am. Chem. Soc. 136 (2014) 13826–13834.
[22] M. Schulze, V. Kunz, P.D. Frischmann, F. Würthner, Nat. Chem. 8 (2016) 576–583.
[23] H. Li, F. Li, B. Zhang, X. Zhou, F. Yu, L. Sun, J. Am. Chem. Soc. 137 (2015) 4332–4335.
[24] C. Panda, J. Debgupta, D. Diaz Diaz, K.K. Singh, S. Sen Gupta, B.B. Dhar, J. Am. Chem. Soc. 136 (2014) 12273–12282.
[25] C.-F. Leung, S.-M. Ng, C.-C. Ko, W.-L. Man, J. Wu, L. Chen, T.-C. Lau, Energy Environ. Sci. 5 (2012) 7903–7907.
[26] E. Pizzolato, M. Natali, B. Posocco, A. Montellano Lopez, I. Bazzan, M. Di Valentin, P. Galloni, V. Conte, M. Bonchio, F. Scandola, A. Sartorel, Chem. Commun. 49 (2013) 9941–9943.
[27] R. Cao, W. Lai, P. Du, Energy Environ. Sci. 5 (2012) 8134–8157.
[28] X. Du, Y. Ding, F. Song, B. Ma, J. Zhao, J. Song, Chem. Commun. 51 (2015) 13925–13928.
[29] L. Yu, X. Du, Y. Ding, H. Chen, P. Zhou, Chem. Commun. 51 (2015) 17443–17446.
[30] F. Evangelisti, R. Guttinger, R. More, S. Luber, G.R. Patzke, J. Am. Chem. Soc. 135 (2013) 18734–18737.
[31] Y. Zhao, J. Lin, Y. Liu, B. Ma, Y. Ding, M. Chen, Chem. Commun. 51 (2015) 17309–17312.
[32] Q. Yin, J.M. Tan, C. Besson, Y.V. Geletii, D.G. Musaev, A.E. Kuznetsov, Z. Luo, K.I. Hardcastle, C.L. Hill, Science 328 (2010) 342–345.
[33] F. Song, Y. Ding, B. Ma, C. Wang, Q. Wang, X. Du, S. Fu, J. Song, Energy Environ. Sci. 6 (2013) 1170–1184.
[34] M. Zheng, Y. Ding, X. Cao, T. Tian, J. Lin, Appl. Catal. B-Environ. 237 (2018) 1091–1100.
[35] D. Hong, J. Jung, J. Park, Y. Yamada, T. Suenobu, Y.-M. Lee, W. Nam, S. Fukuzumi, Energy Environ. Sci. 5 (2012) 7606–7616.
[36] S. Fu, Y. Liu, Y. Ding, X. Du, F. Song, R. Xiang, B. Ma, Chem. Commun. 50 (2014) 2167–2169.
[37] G. Chen, L. Chen, S.M. Ng, T.C. Lau, ChemSusChem 7 (2014) 127–134.
[38] A.M. Ullman, Y. Liu, M. Huynh, D.K. Bediako, H. Wang, B.L. Anderson, D.C. Powers, J.J. Breen, H.D. Abruña, D.G. Nocera, J. Am. Chem. Soc. 136 (2014) 17681–17688.
[39] J.-W. Wang, P. Sahoo, T.-B. Lu, ACS Catal. 6 (2016) 5062–5068.
[40] N.S. McCool, D.M. Robinson, J.E. Sheats, G.C. Dismukes, J. Am. Chem. Soc. 133 (2011) 11446–11449.
[41] S. Berardi, G. La Ganga, M. Natali, I. Bazzan, F. Puntoriero, A. Sartorel, F. Scandola, S. Campagna, M. Bonchio, J. Am. Chem. Soc. 134 (2012) 11104–11107.
[42] B. Schwarz, J. Forster, M.K. Goetz, D. Yücel, C. Berger, T. Jacob, C. Streb, Angew. Chem. Int. Ed. 55 (2016) 6329–6333.
[43] F. Song, R. Moré, M. Schilling, G. Smolentsev, N. Azzaroli, T. Fox, S. Luber, G.R. Patzke, J. Am. Chem. Soc. 139 (2017) 14198–14208.
[44] M. Okamura, M. Kondo, R. Kuga, Y. Kurashige, T. Yanai, S. Hayami, V.K.K. Praneeth, M. Yoshida, K. Yoneda, S. Kawata, S. Masaoka, Nature 530 (2016) 465–468.
[45] J. Xin, L. Jian, Y. Bing, W. Xiang-Zhu, K. Yi, H. Mao-Yong, T. Chen-Ho, W. Li-Zhu, Angew. Chem. Int. Ed. 57 (2018) 7850–7854.
[46] T. Ishizuka, A. Watanabe, H. Kotani, D. Hong, K. Satonaka, T. Wada, Y. Shiota, K. Yoshizawa, K. Ohara, K. Yamaguchi, S. Kato, S. Fukuzumi, T. Kojima, Inorg. Chem. 55 (2016) 1154–1164.
[47] G. Maayan, N. Gluz, G. Christou, Nat. Catal. 1 (2018) 48–54.
[48] S.O.H. Gutschke, D.J. Price, A.K. Powell, P.T. Wood, Angew. Chem. Int. Ed. 38 (1999) 1088–1090.

[49] Z. Huang, Z. Luo, Y.V. Geletii, J.W. Vickers, Q. Yin, D. Wu, Y. Hou, Y. Ding, J. Song, D.G. Musaev, C.L. Hill, T. Lian, J. Am. Chem. Soc. 133 (2011) 2068–2071.

[50] L. Yu, Y. Ding, M. Zheng, H. Chen, J. Zhao, Chem. Commun. 52 (2016) 14494–14497.

[51] Y.V. Geletii, Z. Huang, Y. Hou, D.G. Musaev, T. Lian, C.L. Hill, J. Am. Chem. Soc. 131 (2009) 7522–7523.

[52] J. Wei, Y. Feng, P. Zhou, Y. Liu, J. Xu, R. Xiang, Y. Ding, C. Zhao, L. Fan, C. Hu, ChemSusChem 8 (2015) 2630–2634.

[53] T.C. Davenport, H.S. Ahn, M.S. Ziegler, T.D. Tilley, Chem. Commun. 50 (2014) 6326–6329.

[54] Y.I. Cho, D.M. Joseph, M.J. Rose, Inorg. Chem. 52 (2013) 13298–13300.

[55] R. Al-Oweini, A. Sartorel, B.S. Bassil, M. Natali, S. Berardi, F. Scandola, U. Kortz, M. Bonchio, Angew. Chem. Int. Ed. 53 (2014) 11182–11185.

[56] L. Ma, Q. Wang, W.-L. Man, H.-K. Kwong, C.-C. Ko, T.-C. Lau, Angew. Chem. Int. Ed. 54 (2015) 5246–5249.

[57] D. Wang, J.T. Groves, Proc, Natl. Acad. Sci. U. S. A. 110 (2013) 15579–15584.